nature geoscience

ARTICLES

https://doi.org/10.1038/s41561-019-0408-5

Early continental crust generated by reworking of basalts variably silicified by seawater

Luc André[1,2]*, Kathrin Abraham[3], Axel Hofmann[4], Laurence Monin[1], Ilka C. Kleinhanns[5] and Stephen Foley[6]

The Archaean continental crust comprises two major groups of silicon-rich granitoids: the tonalite–trondhjemite–granodiorite and granite–monzonite–syenite suites, which differ in their sodium-to-potassium ratios. How these felsic granitoids evolved from their mafic precursors remains elusive and the subject of great debate. Here, we present silicon isotopic constraints on the formation of representative trondhjemitic and granitic plutons from the Kaapvaal craton that range in age from 3.51–2.69 billion years ago. We identified very consistent silicon isotopic signatures, all uniformly 0.1–0.2‰ heavier than rocks of the modern continental crust. This unusual composition is explained by the melting of a mafic source that included significant proportions (15–35 wt%) of silicified basalts, which were common supracrustal rocks before 3 billion years ago. Before the melting event that formed the granitoid magmas at depth, portions of the mafic source rocks were enriched in silica by interaction with silica-saturated seawater. The addition of silica depresses the stability of amphibole at similar water activity, allowing trondhjemitic and granitic melt production at lower temperatures from protoliths with contrasting silica contents: 52–57 and ≥60 wt%, respectively. This explains why granitoids were able to form very early in Earth history but did not emerge in significant amounts on other rocky planets.

The Earth is unique among the rocky planets of the solar system in possessing a thick felsic continental crust. Recent models[1–4] are converging to indicate that the continental crust formed relatively early in Earth's history and reached 30–70% of its present volume by 3 billion years ago (Ga), depending on the rate of crustal recycling[4]. Granitoids of the high-Na tonalite–trondhjemite–granodiorite (TTG) and high-K granite–monzonite–syenite (GMS) suites comprise the bulk of this early phase of continental growth. Establishing how these granitoid rocks formed is critical for understanding how the continental crust grew in this early phase and why this phenomenon is unique among the rocky planets. Silicon is the most abundant cation in the Earth's continental crust[5], and its abundance distinguishes the continental crust from the other major Earth reservoirs. Defining the source of silicon in early crustal TTGs and GMSs through a study of their isotopic composition (δ^{30}Si) is therefore a potential way to track how the continents initially formed.

The main modern terrestrial silicate reservoirs have quite similar average Si isotopic compositions. In particular, basaltic melts ($\delta^{30}Si = -0.32 \pm 0.12$‰; average of refs. [6,7]) do not differ from their mantle-source reservoirs (-0.29 ± 0.08‰)[6,8], but their differentiated melts become very slightly enriched in heavy silicon (up to a maximum δ^{30}Si of around −0.14‰) due to the small bulk $\Delta^{30}Si_{solid\text{-}melt}$ isotopic fractionation (around −0.125‰)[9]. Together, these rocks define an 'igneous array' (Fig. 1a), which describes the predicted changes of the Si isotopic composition as a function of the silica content of melts[6,9]. With the exception of sediment-derived peraluminous leucogranites[10,11] and a few andesites[11], all Phanerozoic Si-rich rocks ($SiO_2 > 55$ wt%) fall on this trend (Fig. 1a). In contrast with igneous reservoirs, supracrustal rocks exhibit significant Si isotopic differentiations of up to 10‰ due to large equilibrium and kinetic isotopic fractionations between phases at low temperatures[12,13]. This is the consequence of preferential incorporation of light isotopes (^{28,29}Si) in precipitated secondary minerals[13], biogenic silica[12], and clays in soils and sediments[14], all three of which are counterbalanced by the relative enrichment of ^{30}Si in the water-dissolved silicon fractions. These diverse mineral–fluid interactions converge to make the global hydrosphere the principal terrestrial ^{30}Si-rich reservoir. Hence, silicon isotopes have the great advantage of effectively differentiating between marine authigenic precipitates and the weathering products of silicates.

Precambrian seawater was enriched in Si, which led to widespread deposition of banded iron formations (BIFs) and cherts. These display a wide range of Si isotopic compositions[15,16]: silicon in BIF is usually light (mean δ^{30}Si at −1.1‰[16]), while in cherts it is mostly heavy (mean δ^{30}Si at +0.8‰[16]). Both probably precipitated from a common oceanic reservoir with heavy Si isotopes because of contrasting isotopic fractionations[16]: the combined Fe–Si gel precursors of BIFs[16,17] display $\Delta^{30}Si_{gel\text{-}aqueous}$ (−2.3 to −3.2‰)[16] twice the magnitude of pure Si gels ($\Delta^{30}Si_{gel\text{-}aqueous} = 0$ to −1‰)[16] from which cherts were probably deposited. During the Eoarchaean to Palaeoarchaean, the paucity of emerged continents[18] limited the soil-derived silicon flux to seawater. Instead, oceanic silicon input was mostly from the leaching of Si from oceanic crust by high-temperature hydrothermal alteration[19]. Si input is considered to have been equal to Si removal through the low-temperature hydrothermal silicification of oceanic substrate and the deposition of amorphous silica associated with BIFs and cherts on the seafloor[19]. Because all of these precipitates are enriched in ^{28}Si relative to seawater, by mass balance, this implies that both the remaining Si-saturated seawater and the subsequent precipitated silica would have developed higher δ^{30}Si through time[19]. In parallel, because they reacted with heavy seawater Si, the silicification of Archaean oceanic substrates—

[1]Earth Science Department, Royal Museum for Central Africa, Tervuren, Belgium. [2]Laboratoire G-Time, Département Géosciences, Environnement et Société, Université Libre de Bruxelles, Brussels, Belgium. [3]Tritium Science Group, United Kingdom Atomic Energy Authority, Abingdon, UK. [4]Department of Geology, University of Johannesburg, Johannesburg, South Africa. [5]FB Geowissenschaften—Isotopengeochemie, Universität Tübingen, Tübingen, Germany. [6]Department of Earth and Planetary Sciences, Macquarie University, Sydney, New South Wales, Australia. *e-mail: lucandre@africamuseum.be

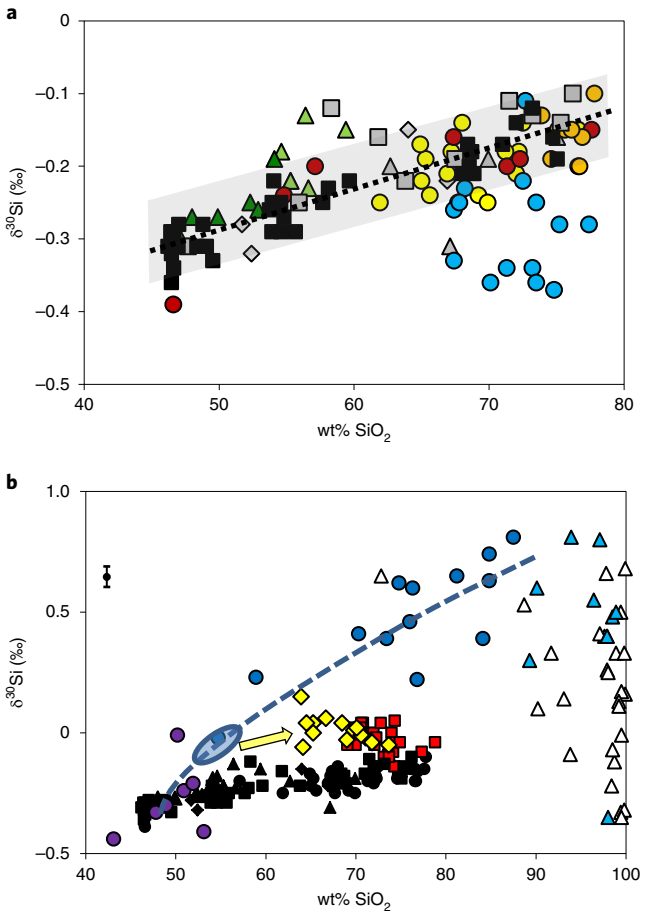

Fig. 1 | Bulk-rock silicon isotopic composition versus SiO_2 content. **a**, The dotted line marks the linear 'igneous array' of the equation '$\delta^{30}Si$ (‰) = 0.0056 × SiO_2 (wt%) −0.567', defined by the differentiation trends of Afar and Iceland[9] (black squares). The grey domain is a 2 s.e.m. uncertainty of ±0.05‰ around that trend line[9]. Most other terrestrial igneous rocks plot within this domain, including: the Cedar Butte volcano differentiation trend from the Snake River[22] (grey squares); the Finland granophyre from the Duluth complex[22] (grey triangles); the Torres del Paine differentiation trend[28] (brown circles); aluminous I-type granites[10,11] (yellow circles); peralkaline A-type granites[10,11] (orange circles); mafic and felsic melts from the granulitic McBride xenoliths[47] (grey diamonds); basalts, gabbro and diorite (dark green triangles); and some calc-alkaline andesites[11] (light green triangles). Peraluminous S-type granites[10,11] (blue circles) constitute a prominent exception, deviating markedly towards low $\delta^{30}Si$. **b**, Silicon isotopic compositions of bulk TTG (yellow diamonds) and GMS (red squares) from the eastern Kaapvaal craton. The samples are consistently heavier than rocks of the terrestrial 'igneous array' (the small black symbols represent all rocks falling on the igneous array shown in **a**). TTGs plot just to the right of the array (dashed blue line), as defined by the mixture between unsilicified (purple circles) and silicified metabasalts (blue circles) and intercalated cherts (blue triangles) from the Onverwacht Group[20]. Other cherts from the Buck Reef Chert of Barberton (white triangles)[48] are plotted for comparison. The elliptic domain between 52 and 57 SiO_2 wt% indicates the composition of the putative source for TTGs as proposed here. The yellow arrow parallel to the igneous array defines the probably positive increases in both $\delta^{30}Si$ and SiO_2 provoked by equilibrium melting of silicified protoliths to produce TTGs. The error bar represents the average 2 s.e.m. error (±0.05‰) on $\delta^{30}Si$ (Methods).

principally basaltic—caused them to acquire bulk positive Si isotopic compositions[20]. Therefore, Si isotopes have a great potential to fingerprint the source of Archaean granitoids by distinguishing between potential contributions from BIFs, shale, igneous rock, silicified basalt and cherts, on a graded scale from negative to positive $\delta^{30}Si$ signatures. A crucial factor is the strong resistance of silicon isotopic signatures to metamorphic equilibration, even at temperatures >700 °C[21]. This implies that supracrustal $\delta^{30}Si$ will survive unchanged to depths where melting might occur[10,11].

Representative granitoid rocks from the vicinity of the Barberton Greenstone Belt (BGB) of the Kaapvaal craton were selected to encompass the Archaean progression from early TTG plutons (3.51–3.11 Ga; mostly trondhjemitic granitoids) to later GMS plutons (3.20–2.69 Ga, mostly K-rich granites). Their normative feldspar compositions are illustrated in Supplementary Fig. 1 and the sample locations are listed in Supplementary Table 1. $\delta^{30}Si$ and $\delta^{29}Si$ for all samples, as well as the pluton ages and some key geochemical features (SiO_2, K_2O/Na_2O, Eu/Eu*, La_N/Yb_N, Sr/Y and Lu/Hf), are summarized in Supplementary Table 2. In terms of their average $\delta^{30}Si$, there are no resolvable differences between TTG and GMS samples at +0.01 ± 0.11‰ (±2 s.d.; n = 15) and −0.03 ± 0.11‰ (±2 s.d.; n = 22), respectively. On a $\delta^{30}Si$ versus SiO_2 diagram (Fig. 1b), they all plot clearly above the 'igneous array', and are significantly heavier than both Phanerozoic I- and A-type granites ($\delta^{30}Si$ = −0.19 ± 0.08‰[10,11]), as well as dacite–rhyolite melts differentiated from basalts ($\delta^{30}Si$ = −0.17 ± 0.08‰[9,22]).

Origin of the heavy Si isotopic signature of TTG

Two main families of models have been proposed for the origin of TTG magmas: (1) melting of metabasalts recycled into the mantle or reworked at the base of a thickened basaltic crust[23]; and (2) fractionation of hydrous basalts[24]. In both cases, garnet and/or amphibole play a key role in shaping the geochemistry of the melts, especially in producing their characteristic fractionations of light from heavy rare-Earth elements (La_N/Yb_N) as well as of Sr relative to Y. Both garnet and amphibole could preferentially incorporate the light Si isotopes relative to quartz[25], and it has been calculated[26] that a melt produced by low-degree melting of eclogite might bear heavier Si isotopic values (−0.13 < $\delta^{30}Si$ < −0.07‰), close to the range of what we observe for the Barberton TTGs. However, because we do not see any variation of $\delta^{30}Si$ as a function of the large variation in La_N/Yb_N (5–68) and Sr/Y (22–228) found in the TTGs (Supplementary Fig. 2a,b), partial melting or fractional crystallization involving garnet or amphibole can be ruled out as the major cause for the recorded heavy $\delta^{30}Si$.

Thermal diffusion is another potential means to provoke changes in Si isotopes, with ^{30}Si being consistently enriched towards the cold end of the system[27]. In this case, the heavy Si isotopic composition of TTGs would be consistent with thermal diffusion-controlled isotopic fractionation, whereby $\delta^{30}Si$ increases with cooling at decreasing depth. However, in the three natural occurrences of felsic rocks where a possible diffusion-related fractionation has been proposed[22,28], the silicon isotopic composition of the felsic components remains within the range of the igneous array (Fig. 1a). Furthermore, if thermal diffusion were to account for the high $\delta^{30}Si$ of the Barberton granitoids, it is unclear why these differ from Phanerozoic granitoids. Our conclusion is that thermal diffusion generates quite limited Si isotopic fractionation and is far from sufficient to account for the observed high $\delta^{30}Si$ values.

Crustal assimilation by granitoid melts of all types is widespread and has to be considered as a plausible cause of the observed heavy $\delta^{30}Si$. Cherts are well represented within the ~18-km-thick Onverwacht Group of the BGB into which several of the studied TTGs intruded[29]. Their variable but generally heavy $\delta^{30}Si$ (Fig. 1b) identifies them as potential contaminants, especially given the presence of chert xenoliths in some TTG plutons[30]. However, most TTGs plot far outside the domain delineated by possible assimilation and fractional crystallization curves[31] for a chert assimilation (Supplementary Fig. 3a,b), which can thus be ruled out as the controlling factor for their high $\delta^{30}Si$.

Basalts from the Onverwacht Group bear average mantle-like signatures ($\delta^{30}Si = -0.30 \pm 0.14‰$ (± 2 s.e.m.))[20], although $\delta^{30}Si$ values are more scattered compared with their modern equivalents due to hydrothermal overprints (Fig. 1b). In contrast, silicified Onverwacht Group seafloor basalts display ^{30}Si-enriched seawater-derived isotopic signatures ($\delta^{30}Si = +0.43 \pm 0.14‰$ (± 2 s.e.m.))[20]. In a $\delta^{30}Si$–SiO_2 diagram (Fig. 1b), Barberton TTGs plot to the right of and below the trend defined by these unsilicified and silicified basalts and associated cherts. This observation supports the hypothesis of TTG derivation by melting of a stack of variably silicified mafic rocks that were geodynamically placed into appropriate pressure–temperature conditions for melting. This is because the melting process would produce liquids enriched in silica with only limited Si isotopic fractionations (~0.1‰)[9], pushing the data laterally to the right of the silicified basalt trend. It is worth mentioning that all early Archaean rocks exposed to seafloor conditions (including ultramafic and felsic volcanics) were prone to silicification[29], but we focus our discussion on basalts because they are the most common rocks in greenstone belts[32]. Cherts must have been part of the mixture of rocks that melted, but only to a small extent, because they are both volumetrically minor and relatively infertile compared with silicified basalts. Since their average Si isotopic composition ($\delta^{30}Si = +0.39 \pm 0.17‰$ (± 2 s.e.m.))[20] overlaps with that of the silicified basalts (Fig. 1b), any contribution from the cherts is effectively included in the weighted average of silicified basalts.

Since the metabasalts of the Theespruit Formation (~3.54 Ga) incorporate the oldest silicified rocks at the base of the Onverwacht Group and predate all studied TTGs (3.51–3.11 Ga), they can be regarded as a suitable source type. Using their average compositions of silicified and unsilicified metabasalts as potential mixing end members (Supplementary Table 3), mixtures including about 15–35% of silicified metabasalts (one for every three parts on average) account for TTG's properties (both its K_2O/Na_2O ratio and its $\delta^{30}Si$ values) (Supplementary Fig. 4). This range equals about 52–57 SiO_2 wt% in the TTG protoliths. Using phase equilibria modelling, Johnson et al.[33] constrained the origin of TTGs from the Pilbara craton as produced by 20–30% melting of low-MgO tholeiites of the ~3.5 Ga Coucal Formation from the Pilbara Supergroup. Our proposed mixture incorporating approximately 1:3 proportions of silicified and unsilicified Theespruit metabasalts has a major element composition similar to the average Coucal basalt (C-F2; Supplementary Table 3). In particular, its low MgO content (5.6 wt%) supports this 1:3 assemblage as a suitable source rock from which TTG-like melts could be extracted at realistic geothermal gradients (700–1,100 °C GPa^{-1})[33].

All Theespruit metabasalts have low Lu/Hf values (Fig. 2), which is again similar to the Coucal basalt (0.12; Supplementary Table 3). This is another key point, because a source with such a low Lu/Hf ratio relative to normal mid-ocean ridge basalts (N-MORBs; 0.195) is necessary to account for the very low Lu/Hf characteristics (0.035 on average) of early Earth TTGs[34,35]. This is probably the consequence of the preferential depletion of Lu relative to Hf during Archaean basalt alteration[29], which is especially amplified in most silicified portions of the Onverwacht Group with the highest $\delta^{30}Si$ (Fig. 2). Therefore, we are confident that ~1:3 mixture of silicified and unsilicified Theespruit metabasalts constitutes a robust source rock for all Barberton TTGs.

Silicifying a metabasalt source promotes TTG melts

Rocks with higher SiO_2 contents have more restricted amphibole stability at similar water activity[36]. Since TTG-like Archaean crust probably formed by the melting of garnet amphibolite[37], the addition of free quartz in the mafic protolith permits melting at lower temperatures ($\Delta T = \sim 100$ °C)[38,39], at the relatively low MgO content[33] that results from silicification. This promotes TTG production earlier in Earth's history when the MgO-rich crust would have

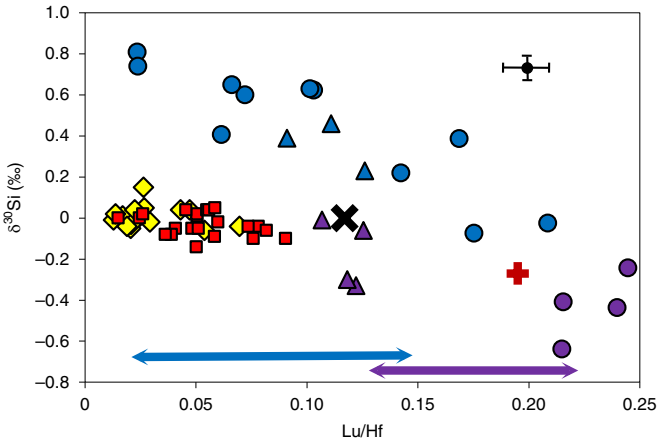

Fig. 2 | $\delta^{30}Si$ versus Lu/Hf. $\delta^{30}Si$ and Lu/Hf data for Theespruit (triangles) and Hooggenoeg–Kromberg (circles) silicified (blue) and unsilicified (purple) metabasalts were taken from refs. [20,29], respectively. The N-MORB (brown cross) Lu/Hf and $\delta^{30}Si$ values are from refs. [6,49], respectively. Lu/Hf ratios decreased as a consequence of silicification[29]. This is apparent in the decrease of Lu/Hf as a function of the increase in $\delta^{30}Si$, while corresponding La/Nb and Th/Nb ratios remained undisturbed and in the close range of fresh N-MORBs (Supplementary Table 3). This is confirmed by the range of Lu/Hf ratios (± 1 s.d.) observed in another large dataset of silicified ($SiO_2 > 60$ wt%; Lu/Hf = 0.084 ± 0.062; $n = 16$; blue arrow) and unsilicified ($SiO_2 < 60$ wt%; Lu/Hf = 0.174 ± 0.045; $n = 81$; purple arrow) Onverwacht Group basalts[50]. The low Lu/Hf value of the proposed TTG source (oblique black cross) is in accordance with the low Lu/Hf features of TTG and GMS from the BGB (symbols as in Fig. 1b). The error bars represent the average 2 s.e.m. error ($\pm 0.05‰$) on $\delta^{30}Si$ and a reproducibility confidence of ± 0.01 units on the Lu/Hf ratio (Methods).

otherwise been incapable of producing TTG melts[37]. The enhanced fertility is proposed to occur via the fluid-absent breakdown of amphibole + plagioclase + quartz to produce a peritectic assemblage of garnet-pyroxenes with melts[39]. As such, the addition of quartz causes plagioclase to be a reactant, leaving more Na available for incorporation into the TTG-like melt. Importantly, this boosted fertility ceases when free quartz is exhausted from the assemblage[39]. This would have applied to the silicified mafic source considered here with 52–57 wt% SiO_2, whereas the melting of amphibolites with still higher SiO_2 (60 wt%) would have generated granodioritic–granitic melts with K/Na ratios higher than trondhjemites[38]. Hence, anatexis to produce TTG melts probably requires silicified metabasalts carrying relatively low silica contents (blue elliptic domain in Fig. 1b). During equilibrium melting, we expect isotopically heavier melts, balanced by isotopically lighter restites (yellow arrow in Fig. 1b). However, if an isotopic disequilibrium arises through rapid melt extraction following the dehydration melting of $\delta^{30}Si$-light amphiboles triggered by the $\delta^{30}Si$-heavy quartz comsumption[39], melt $\delta^{30}Si$ might be either slightly lighter or heavier than the initial composition of the protolith, depending of the amphibole-to-quartz ratio involved in the melt.

Origin of the heavy Si isotopic signature of GMS

Two major mechanisms have been invoked to explain the origin of K-rich GMS melts: (1) melting of older TTG gneisses[30,35]; and (2) partial melting of enriched tholeiites[33]. The high $\delta^{30}Si$ values of most GMSs (close to the TTG range) appear to be straightforward evidence in favour of their derivation from the melting of a TTG-rich protocrust. However, the relationships between pluton ages, their $\delta^{30}Si$ values and Eu anomalies (Fig. 3) indicate that a clear distinction needs to be made between most of the older (≥3.11 Ga)

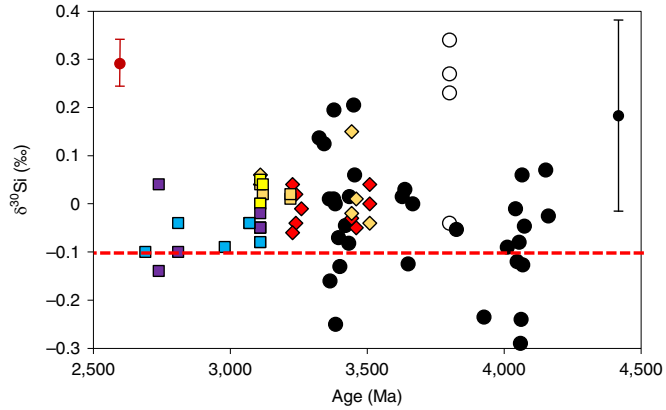

Fig. 3 | Hadean–Archaean δ^{30}Si granitoid signatures. This δ^{30}Si versus age diagram compares the TTG (diamonds) and GMS data (squares) from this study with compositionally different layers from the Amîtsoq gneiss[21] (white circles) and estimated δ^{30}Si values of pre-3.3 Ga felsic rocks (black circles) from which detrital Jack Hills zircons[42] originate. Note that the black error bar for secondary ion mass spectrometer zircon δ^{30}Si values is larger (±0.2‰)[42] than the brown one for MC-ICP-MS bulk-rock δ^{30}Si values (±0.05‰). TTG and GSM samples are colour coded depending on their Eu anomaly (red, Eu/Eu* > 1.0; orange, 0.8 < Eu/Eu* < 1.0; yellow, 0.6 < Eu/Eu* < 0.8; purple, 0.4 < Eu/Eu* < 0.6; blue, Eu/Eu* < 0.4). The dashed red line represents the upper limit (around −0.1‰) of the igneous array at 75 wt% SiO_2. All rocks above this threshold are regarded to carry a significant proportion of seawater-derived Si in their protoliths.

K-rich granites (Dalmein, Nelspruit, Piggs Peak and Salisbury Kop plutons), which bear very similar δ^{30}Si, Eu/Eu* (>0.7) and Sr/Y (13–53; Supplementary Fig. 2b) values to TTGs, and the younger (~3.1–2.69 Ga) GMS intrusions, which have slightly lighter δ^{30}Si signatures, significantly more negative Eu anomalies (<0.6) and lower Sr/Y ratios (<10; Supplementary Fig. 2b). Partial melting of a TTG-like source should be characterized by large proportions (>45 wt%)[35] of residual plagioclase left after the extraction of the felsic melts. Older GMSs with small or no Eu anomalies are inconsistent with such plagioclase-rich residues. For this reason we speculate that the older K-rich granites continued to tap a heavy δ^{30}Si silicified metabasalt-like reservoir, but with overall higher K_2O/Na_2O ratios coupled with higher silica (>60 wt%) contents (which promotes high K/Na in the melt[38]) than our proposed source for the trondhjemitic melts. Conversely, the younger K-rich granitoids probably record the melting of a pre-existing TTG-like felsic crust. Micas are known to be enriched in ^{28}Si with respect to feldspar (with a $\Delta^{30}Si_{Mica\text{-}feldspar}$ of about −0.3‰) in a tonalitic composition[21]. Therefore, the trend to lighter δ^{30}Si signatures seen in younger GMSs may merely reflect disequilibrium mineral melt segregation, if melt fertility were controlled by rapid dehydration melting of mica with a sluggish diffusion-restricted Si availability from heavier residual plagioclases.

Implications for the Hadean–Archaean record

Our results suggest that the intense silicification of mafic lavas, which was ubiquitous on the Archaean seafloor before 3.0 Ga, played a major role in the generation of the granitoids that formed the early felsic continental crust on Earth. This confirms the importance of feedbacks between surface and deep Earth processes during the Palaeoarchaean and earlier times. Accordingly, we infer a genetic link between the reworking of silicified mafic protoliths at depth and extensive Si enrichment of the Kaapvaal subcontinental lithospheric mantle about 3.3 Ga ago[40]. Although similar seawater-derived silicon recycling at depth has been detected on a much smaller isotopic scale in some Phanerozoic andesites[11], its effect on the Archaean TTGs and GMSs is an order of magnitude larger, reflecting the large-scale 'non-uniformitarian' silicification of Archaean supracrustal rocks, which contrasts with the scarcity of silicification on modern seafloors. This typically Archaean alteration style is accompanied by extensive element redistributions[29], many of which differ from element depletion–enrichment patterns observed during modern-day interactions between seawater and oceanic crust. The substantial lowering of Lu/Hf ratios by silicification appears as a diagnostic characteristic of this non-uniformitarian alteration (Fig. 2), because it strongly contrasts with the lack of Lu/Hf disturbance by modern seafloor alteration processes[41].

A potential caveat to our findings is that all of the data come from the Kaapvaal craton in southern Africa; hence, there could be a geographical bias. However, the various constituent layers (Qz feldspar-, amphibole- and mica-rich layers) of the tonalitic Amîtsoq Gneiss from 3.8 Ga (Isua, West Greenland) exhibit similar heavy δ^{30}Si values[21] (Fig. 3). Besides, Trail et al.[42] recently proposed that Hadean–Archaean detrital zircons extracted from the Jack Hills metaconglomerate (Yilgarn craton, Western Australia) bear seawater-derived Si isotopic signatures. Zircons are enriched in ^{28}Si relative to whole rocks[43], with a $\Delta^{30}Si_{WR\text{-}zircon}$ of about +0.35‰ for tonalitic felsic systems[42]. Applying this fractionation factor to the Jack Hills δ^{30}Si database of detrital zircons[42], we can evaluate the δ^{30}Si of felsic whole rocks from which they were eroded. Most are in the range of the Barberton TTGs (Fig. 3), revealing that most felsic rocks from the early Archaean (and possibly the Hadean) might carry similar proportions of seawater-derived silicon. This highlights the probable global significance of reworked silicified seafloor protoliths as an essential element to generate the primordial felsic nuclei of continental crust.

By linking the primeval growth of silicic crust to the evolution of seawater–seafloor interactions on the early Earth, we implicitly address the question of why granitoid rocks are rare or absent on other rocky planets, in particular in the Martian crust, which is mostly basaltic (~50 wt% SiO_2) with few rock types perhaps petrographically reminiscent of TTGs[44]. With the rapid disappearance of an early ocean around 4.1–3.7 Ga[45,46], Mars lacked a surficial Si-saturated water reservoir that would have been able to interact with its basaltic crust for a sufficiently long time period. The absence or restricted scale of such interactions prevented the silicification of Martian mafic rocks that would have been essential, following their subsequent transport to depth, to trigger the formation of a thick TTG-like protocrust.

Online content

Any methods, additional references, Nature Research reporting summaries, source data, statements of code and data availability and associated accession codes are available at https://doi.org/10.1038/s41561-019-0408-5.

Received: 27 November 2018; Accepted: 13 June 2019;
Published online: 26 August 2019

References

1. Belousova, E. A. et al. The growth of the continental crust: constraints from zircon Hf-isotope data. *Lithos* **119**, 457–466 (2010).
2. Dhuime, B., Hawkesworth, C. J., Delavault, H. & Cawood, P. A. Continental growth seen through the sedimentary record. *Sediment. Geol.* **357**, 16–32 (2017).
3. Pujol, M., Marty, B., Burgess, R., Turner, G. & Philippot, P. Argon isotopic composition of Archaean atmosphere probes early Earth geodynamics. *Nature* **498**, 87–90 (2013).
4. Rosas, J. C. & Korenaga, J. Rapid crustal growth and efficient crustal recycling in the early Earth: implications for Hadean and Archean geodynamics. *Earth Planet. Sci. Lett.* **494**, 42–49 (2018).
5. Taylor, S. R. Abundance of chemical elements in the continental crust: a new table. *Geochim. Cosmochim. Acta* **28**, 1273–1285 (1964).
6. Savage, P. S., Armytage, R. M. G., Georg, R. B. & Halliday, A. E. High temperature silicon isotope geochemistry. *Lithos* **190–191**, 500–519 (2014).

7. Pringle, E. A. et al. Silicon isotopes reveal recycled altered oceanic crust in the mantle sources of ocean island basalts. *Geochim. Cosmochim. Acta* **189**, 282–295 (2016).
8. Savage, P. S., Georg, R. B., Armytage, R. M. G., Williams, H. M. & Halliday, A. N. Silicon isotope homogeneity in the mantle. *Earth Planet. Sci. Lett.* **295**, 139–146 (2010).
9. Savage, P. S., Georg, R. B., Williams, H. M., Burton, K. W. & Halliday, A. N. Silicon isotope fractionation during magmatic differentiation. *Geochim. Cosmochim. Acta* **75**, 6124–6139 (2011).
10. Savage, P. S. et al. The silicon isotope composition of granites. *Geochim. Cosmochim. Acta* **92**, 184–202 (2012).
11. Poitrasson, F. & Zambardi, T. An Earth–Moon silicon isotope model to track silicic magma origins. *Geochim. Cosmochim. Acta* **167**, 301–312 (2015).
12. Frings, P. J., Clymans, W., Fontorbe, G., De La Rocha, C. L. & Conley, D. J. The continental Si cycle and its impact on the ocean Si isotope budget. *Chem. Geol.* **425**, 12–36 (2016).
13. Kleine, B. I., Stefánsson, A., Halldórsson, S. A., Whitehouse, M. J. & Jónasson, K. Silicon and oxygen isotopes unravel quartz formation processes in the Icelandic crust. *Geochem. Persp. Lett.* **7**, 5–11 (2018).
14. Bayon, G. et al. The silicon isotopic composition of fine-grained river sediments and its relation to climate and lithology. *Geochim. Cosmochim. Acta* **229**, 147–161 (2018).
15. Chakrabarti, R., Knoll, A. H., Jacobsen, S. B. & Fischer, W. W. Si isotope variability in Proterozoic cherts. *Geochim. Cosmochim. Acta* **91**, 187–201 (2012).
16. Zheng, X.-Y., Beard, B. L., Reddy, T. R., Roden, E. E. & Johnson, C. M. Abiologic silicon isotope fractionation between aqueous Si and Fe(III)–Si gel in simulated Archean seawater: implications for Si isotope records in Precambrian sedimentary rocks. *Geochim. Cosmochim. Acta* **187**, 102–122 (2016).
17. Delvigne, C., Cardinal, D., Hofmann, A. & André, L. Stratigraphic changes of Ge/Si, REE + Y and silicon isotopes as insights into the deposition of a Mesoarchaean banded iron formation. *Earth Planet. Sci. Lett.* **355–356**, 109–118 (2012).
18. Cawood, P. A. & Hawkesworth, C. J. Continental crustal volume, thickness and area, and their geodynamic implications. *Gondwana Res.* **66**, 116–125 (2019).
19. Marin-Carbonne, J., Robert, F. & Chaussidon, M. The silicon and oxygen isotope compositions of Precambrian cherts: a record of oceanic paleo-temperatures? *Precambr. Res* **247**, 223–234 (2014).
20. Abraham, K. et al. Coupled silicon–oxygen isotope fractionation traces Archaean silicification. *Earth Planet. Sci. Lett.* **301**, 222–230 (2011).
21. André, L., Cardinal, D., Alleman, L. Y. & Moorbath, S. Silicon isotopes in ~3.8 Ga West Greenland rocks as clues to the Eoarchaean supracrustal Si cycle. *Earth Planet. Sci. Lett.* **245**, 162–173 (2006).
22. Zambardi, T., Lundstrom, C. C., Li, X. & McCurry, M. Fe and Si isotope variations at Cedar Butte volcano; insight into magmatic differentiation. *Earth Planet. Sci. Lett.* **405**, 169–179 (2014).
23. Rapp, R. P. & Watson, E. B. Dehydratation melting of metabasalt at 8–32 kbar: implications for continental growth and crust–mantle recycling. *J. Petrol.* **36**, 891–931 (1995).
24. Kleinhanns, I. C., Kramers, J. D. & Kamber, B. S. Importance of water for Archaean granitoid petrology: a comparative study of TTG and potassic granitoids from Barberton Mountain Land, South Africa. *Contrib. Mineral. Petrol.* **145**, 377–389 (2003).
25. Méheut, M. & Schauble, E. A. Silicon isotope fractionation in silicate minerals: insights from first-principles models of phyllosilicates, albite and pyrope. *Geochim. Cosmochim. Acta* **134**, 137–154 (2014).
26. Yu, H.-M., Li, Y.-H., Gao, Y.-J., Huang, J. & Huang, F. Silicon isotopic compositions of altered oceanic crust: implications for Si isotope heterogeneity in the mantle. *Chem. Geol.* **479**, 1–9 (2018).
27. Richter, F. M. et al. Isotopic fractionation of the major elements of molten basalt by chemical and thermal diffusion. *Geochim. Cosmochim. Acta* **73**, 4250–4263 (2009).
28. Gajos, N. A., Lundstrom, C. C. & Taylor, A. H. Spatially controlled Fe and Si isotope variations: an alternative view on the formation of the Torres del Paine pluton. *Contrib. Mineral. Petrol.* **171**, 93 (2016).
29. Hofmann, A. & Harris, C. Silica alteration zones in the Barberton Greenstone Belt: a window into subseafloor processes 3.5–3.3 Ga ago. *Chem. Geol.* **257**, 221–239 (2008).
30. Agangi, A., Hofmann, A. & Elburg, M. A. A review of Palaeoarchaean felsic volcanism in the eastern Kaapvaal craton: linking plutonic and volcanic records. *Geosci. Front.* **9**, 667–688 (2018).
31. DePaolo, D. J. Trace element and isotopic effects of combined wallrock assimilation and fractional crystallization. *Earth Planet. Sci. Lett.* **53**, 189–202 (1981).
32. Smithies, R. H. et al. Two distinct origins for Archean greenstone belts. *Earth Planet. Sci. Lett.* **487**, 106–116 (2018).
33. Johnson, T. E., Brown, M., Gardiner, N. J., Kirkland, C. L. & Smithies, R. H. Earth's first stable continents did not form by subduction. *Nature* **543**, 239–242 (2017).
34. Blichert-Toft, J. & Albarède, F. Hafnium isotopes in Jack Hills zircons and the formation of the Hadean crust. *Earth Planet. Sci. Lett.* **265**, 686–702 (2008).
35. Gardiner, N. J., Johnson, T. E., Kirkland, C. L. & Smithies, R. H. Melting controls on the lutetium–hafnium evolution of Archaean crust. *Precam. Res.* **305**, 479–488 (2018).
36. Gilbert, M. C., Helz, R. T., Popp, R. K. & Spear, F. S. in *Reviews in Mineralogy, Volume 9b, Amphiboles: Petrology and Experimental Phase Relations* (eds Veblen, D. R. & Ribbe, P. H.) 229–353 (Mineralogical Society of America, 1982).
37. Foley, S. F., Buhre, S. & Jacob, D. E. Evolution of the Archaean crust by delamination and shallow subduction. *Nature* **421**, 249–252 (2003).
38. Patiño Douce, A. E. & Beard, J. S. Dehydration-melting of biotite gneiss and quartz amphibolite from 3 to 15 kbar. *J. Petrol.* **36**, 707–738 (1995).
39. Stuck, T. J. & Diener, J. F. A. Mineral equilibria constraints on open-system melting in metamafic compositions. *J. Metamorph. Geol.* **36**, 255–281 (2018).
40. Van der Meer, Q. H. A., Klaver, M., Reisberg, L., Riches, A. J. V. & Davies, G. R. Preservation of an Archaean whole rock Re–Os isochron for the Venetia lithospheric mantle: evidence for rapid crustal recycling and lithosphere stabilisation at 3.3 Ga. *Geochim. Cosmochim. Acta* **216**, 242–263 (2017).
41. Thompson, P. M. E., Kempton, P. D. & Kerr, A. C. Evaluation of the effects of alteration and leaching on Sm–Nd and Lu–Hf systematics in submarine mafic rocks. *Lithos* **104**, 164–176 (2008).
42. Trail, D. et al. Origin and significance of Si and O isotope heterogeneities in Phanerozoic, Archean, and Hadean zircon. *Proc. Natl Acad. Sci. USA* **115**, 10287–10292 (2018).
43. Qin, T., Wu, F., Wu, Z. & Huang, F. First-principles calculations of equilibrium fractionation of O and Si isotopes in quartz, albite, anorthite, and zircon. *Contrib. Mineral. Petrol.* **171**, 91 (2016).
44. Sautter, V. et al. In situ evidence for continental crust on early Mars. *Nat. Geosci.* **8**, 605–609 (2015).
45. Fawdon, P. et al. The Hypanis Valles delta: the last highstand of a sea on early Mars? *Earth Planet. Sci. Lett.* **500**, 225–241 (2018).
46. Rickman, H. et al. Water in the history of Mars: an assessment. *Planet. Space Sci.* **166**, 70–89 (2019).
47. Savage, P. S., Georg, R. B., Williams, H. M. & Halliday, A. N. Silicon isotopes in granulite xenoliths: insights into isotopic fractionation during igneous processes and the composition of the deep continental crust. *Earth Planet. Sci. Lett.* **365**, 221–231 (2013).
48. Geilert, S., Vroon, P. Z. & van Bergen, M. J. Silicon isotopes and trace elements in chert record early Archean basin evolution. *Chem. Geol.* **386**, 133–142 (2014).
49. Gale, A., Dalton, C. A., Langmuir, C. H., Su, Y. & Schilling, J.-G. The mean composition of ocean ridge basalts. *Geochem. Geophy. Geosy.* **14**, 489–518 (2013).
50. Furnes, H., Robins, B. & De Wit, M. J. Geochemistry and petrology of lavas in the upper Onverwacht suite, Barberton Mountain Land, South Africa. *S. Afr. J. Geol.* **115**, 171–210 (2012).

Acknowledgements

We acknowledge E. Ponzevera and G. Bayon (IFREMER, Brest, France) for careful help with the duplicate Neptune MC-ICP-MS analyses of a few specimens. We thank N. Mattielli and J. Dejong for maintenance and precious help during isotopic measurements on the Nu Plasma 2 MC-ICP-MS. This project was supported by the Belgium F.R.S-FNRS 'Grand Equipement—Infrastructure' (number 2.5016.12).

Author contributions

L.A. and S.F. conceived the project. L.M., L.A. and K.A. performed the Si isotope analyses. L.A. interpreted the Si isotope analyses, with help from S.F., A.H. and K.A. L.A. wrote the manuscript, with help from S.F. and A.H. K.A., I.C.K. and A.H. provided input to the fieldwork and petrology.

Competing interests

The authors declare no competing interests.

Additional information

Supplementary information is available for this paper at https://doi.org/10.1038/s41561-019-0408-5.

Reprints and permissions information is available at www.nature.com/reprints.

Correspondence and requests for materials should be addressed to L.A.

Publisher's note: Springer Nature remains neutral with regard to jurisdictional claims in published maps and institutional affiliations.

Methods

Silicon isotopes. Silicon was concentrated from 5 mg of powdered sample digested with 0.2 g analytical-grade NaOH into carbon SIGRADUR crucibles at 730 °C for 10 min in a muffle furnace. The fusion beads were dissolved in 50 ml bi-distilled 0.01 M HNO_3 to obtain an Si stock solution sufficiently dilute to avoid silicic acid polymerization. The acidified solution at a pH of ~2 was recommended[51] for the complete dissolution of Fe-oxyhydroxides and a quantitative elution yield without Si isotopic fractionation during the following purification step. The sample solution was eluted on 1.8-ml Bio-Rad AG 50W-X12 (200–400 mesh; hydrogen form) cation exchange resin, conditioned with different HCl and HNO_3 pre-cleaning and Milli-Q water rinse steps[52]. Some 3 ml of ~60 µg Si was loaded on the column and eluted with 2 ml Milli-Q water. Although the speciation of dissolved Si in water is pH dependent, it occurs as neutral or anionic species at low to neutral pH and thus is not retained by the resin, whereas cationic matrix elements are efficiently retained. The final solution of ~10 ppm Si was directly acidified to 0.14 M HNO_3 for isotope analyses. The reference standards were prepared according to the same method, in parallel with the specimens. Quantitative recovery of Si for the whole method was 99 ± 4%. The full chemical preparation was replicated three or four times on all samples, starting from the rock powders to check the reproducibility of the chemical procedure.

Si isotopic compositions were measured using a Nu Plasma II multicollector inductively coupled plasma mass spectrometer (MC-ICP-MS) in dry plasma mode using the CETAC Aridus II desolvator at the Université Libre de Bruxelles, following published methodologies[53]. The sample introduction system was equipped with a CETAC C-Flow PFA concentric nebulizer with an uptake rate of 100 µl min^{-1}. The membrane and spray chamber of desolvator were cleaned with 10% *v*/*v* warm (70 °C) HNO_3 and dried with isopropanol on argon gas flush to eliminate any residues that may compromise the analyses by memory effect and/or high background. The instrumental mass bias and drift were corrected both by external Mg doping, applying the exponential mass bias law, and by the standard-sample bracketing method[54]. To resolve all molecular interferences ($^{28}SiH^+$, $^{14}N_2^+$ and $^{14}N^{16}O^+$), the measurements were performed at pseudo-high resolution on the interference-free lower mass side of the plateau of flat-top peaks setting with an offset next to mid-slope. A single analysis consisted of three blocks of 20 runs with a 5 s integration time by run on each Si and Mg isotope, separated by 2 s to allow the parameter switch in dynamic mode. The average within-run reproducibility was 0.14‰ (2 s.d.). Typical Si sensitivity was ~20 V ppm^{-1} with a 500–1,000 signal-to-blank ratio, which represents a four- to sixfold improvement compared with our earlier published conditions (125 < signal/blank < 175)[53]. The Mg doping concentration was adjusted to 0.4 ppm Mg for 1 ppm Si to have the Si/Mg voltage ratio close to 1.

Nine specimens using the same total chemical procedure replicated four times were analysed with two different mass spectrometers. Two powder solutions were measured three times each with the Université Libre de Bruxelles Nu instrument following the aforementioned procedure. The remaining two powder solutions were run three times each with a Neptune MC-ICP-MS at the Pôle Spectrométrie Ocean (Brest), using an APEX desolvation unit and medium mass resolution mode, and following the methodology described in ref. [14]. The gap ($\Delta_{Nu\text{-}Neptune}$) between the mean of both groups of measurements varies between 0.02 and 0.08‰, with a mean of 0.04‰ (Supplementary Table 4). This provides an important analytical validation of our in-house determinations and shows the optimal character of six repetitions on two powder aliquots. Hence, we could routinely use the value of two standard errors of the mean (2 s.e.m.) of six total replicates (two duplicates of three powder aliquots; see Supplementary Table 2) as a correct estimate of how far the sample mean of the data is likely to be from the true population mean, with a probability of 95%. This is the external error associated with each measurement listed in Supplementary Table 2. On average, it is ±0.03 and ±0.05‰ for $\delta^{29}Si$ and $\delta^{30}Si$, respectively.

Data are reported as δ values in per mil relative to the international NBS-28 silica standard. Several external standards (GA granite, BHVO-2 basalt and diatomite) were regularly measured during each analytical session. The long-term reproducibilities for $\delta^{30}Si$ obtained on these three standards and given by 2 s.d. over 2-year measurements were of 0.16‰ (n = 76), 0.18‰ (n = 37) and 0.19‰ (n = 88), respectively. Our results gave a mean $\delta^{30}Si$ value of −0.24 ± 0.02‰ (2 s.e.m.; n = 76) for GA granite, −0.29 ± 0.03‰ (2 s.e.m.; n = 37) for BHVO-2 and +1.26 ± 0.02‰ (2 s.e.m.; n = 88) for diatomite. They are all in very good agreement within the uncertainties of the previous measurements, the references of which are given in the Supplementary Table 2. All granitoid samples and the standards analysed in this study define, within error, a good terrestrial mass-dependent fractionation law ($\delta^{29}Si = 0.5095 \times \delta^{30}Si$; Supplementary Fig. 5a,b), which is consistent with equilibrium (slope: $0.5178\delta^{30}Si$) or kinetic (slope: $0.5092\delta^{30}Si$) mass-dependent fractionations.

Major and trace element compositions for specimens 99/xxx are reported in ref. [24]. Major and trace element compositions for specimens BAR 1–10 were obtained by X-ray fluorescence (major elements) and ICP-MS (trace elements) at the University of Mainz, Germany, and followed standard procedures[55]. Data for SW5–1 and MG18/MG35 are reported in refs. [56,57], respectively. For BAR11-16, SINC1 and SINC2, major element contents were determined as reported in ref. [57], while trace elements where analysed by ACME Laboratories in Vancouver, Canada, using ICP-MS following lithium borate fusion. The quality of data was monitored using in-house standard SO-19. For the analyses in this paper, precision was better than 10% except for Be, Cs and Lu (better than 23, 18 and 13%, respectively), on the basis of two repeat analyses of the standard. Accuracy was better than 10% for all elements except Be (better than 23%). Detection limits were typically below 0.1 ppm for rare-earth elements, and below 1 ppm for all other elements except V (below 8 ppm). Previously unpublished results are compiled in Supplementary Table 5.

Data availability

The data supporting the findings of this study are available within the article and its Supplementary Information files.

References

51. Fitoussi, C., Bourdon, B., Kleine, T., Oberli, F. & Reynolds, B. C. Si isotope systematics of meteorites and terrestrial peridotites: implications for Mg/Si fractionation in the solar nebula and for Si in the Earth's core. *Earth Planet. Sci. Lett.* **287**, 77–85 (2009).
52. Georg, R. B., Reynolds, B. C., Frank, M. & Halliday, A. N. New sample preparation techniques for the determination of Si isotopic compositions using MC-ICPMS. *Chem. Geol.* **235**, 95–104 (2006).
53. Abraham, K. et al. $\delta^{30}Si$ and $\delta^{29}Si$ determinations on USGS BHVO-1 and BHVO-2 reference materials with a new configuration on a Nu Plasma multi-collector ICP-MS. *Geostand. Geoanal. Res.* **32**, 193–202 (2008).
54. Cardinal, D., Alleman, L. Y., De Jong, J., Ziegler, K. & André, L. Isotopic composition of silicon measured by multicollector plasma source mass spectrometry in dry plasma mode. *J. Anal. Spectrom.* **18**, 213–218 (2003).
55. Nehring, F., Jacob, D. E., Barth, M. G. & Foley, S. F. Laser-ablation ICP-MS analysis of siliceous rock glasses fused on an iridium strip heater using MgO dilution. *Microchim. Acta* **160**, 153–163 (2008).
56. Hofmann, A. et al. The Nhlangano gneiss dome in south-west Swaziland—a record of crustal destabilization of the eastern Kaapvaal craton in the Neoarchaean. *Precambr. Res.* **258**, 109–132 (2015).
57. Dlamini, N. et al. Supracrustal gneisses in southern Swaziland: a basalt–sandstone assemblage of the upper Mozaan Group deformed in the Neoarchaean. *S. Afr. J. Geol.* **120**, 477–498 (2017).